Queensland University of Technology
Brisbane Australia

This is the author's version of a work that was submitted/accepted for publication in the following source:

Thiyahuddin, Izzat, Gu, YuanTong, Gover, Rory, & Thambiratnam, David (2014) Fluid-structure interaction analysis of full scale vehicle-barrier impact using coupled SPH-FEA. *Engineering Analysis with Boundary Elements*, *42*, pp. 26-36.

This file was downloaded from: http://eprints.qut.edu.au/63968/

© Copyright 2013 Elsevier

This is the author's version of a work that was accepted for publication in Engineering Analysis with Boundary Elements. Changes resulting from the publishing process, such as peer review, editing, corrections, structural formatting, and other quality control mechanisms may not be reflected in this document. Changes may have been made to this work since it was submitted for publication. A definitive version was subsequently published in Engineering Analysis with Boundary Elements, [VOL 42, (2014)] DOI: 10.1016/j.enganabound.2013.10.007

Notice: *Changes introduced as a result of publishing processes such as copy-editing and formatting may not be reflected in this document. For a definitive version of this work, please refer to the published source:*

http://dx.doi.org/10.1016/j.enganabound.2013.10.007

Fluid-Structure Interaction Analysis of Full Scale Vehicle-Barrier Impact using Coupled SPH-FEA

Thiyahuddin M.I[1], Gu Y.T[1*], Gover R.B[1], Thambiratnam D.P[2]

[1]*School of Chemistry, Physics and Mechanical Engineering, Science and Engineering Faculty*
Queensland University of Technology, Brisbane, Queensland, Australia
**Corresponding author's email: yuantong.gu@qut.edu.au*

[2]*School of Civil Engineering and Built Environment, Science and Engineering Faculty*
Queensland University of Technology, Brisbane, Queensland, Australia
email: d.thambiratnam@qut.edu.au

Abstract: Portable water-filled barriers (PWFB) are roadside structures used to separate moving traffic from work-zones. Numerical PWFB modelling is preferred in the design stages prior to actual testing. This paper aims to study the fluid-structure interaction of PWFB under vehicular impact using several methods. The strategy to treat water as non-structural mass was proposed and the errors were investigated. It was found that water can be treated with the FEA-NSM model for velocities higher than 80kmh^{-1}. However, full SPH/FEA model is still the best treatment for water and necessary for lower impact velocities. The findings in this paper can be used as guidelines for modelling and designing PWFB.

Keywords: Coupled Analysis, SPH, Plastic Road Safety Barriers, Impact, Non-structural Mass

1. INTRODUCTION

Portable water-filled barriers (PWFBs) are temporary roadside appurtenances used to keep errant vehicles from penetrating into impermanent work zones on roadways. These barriers are in the semi-rigid group of roadside barriers. Unfilled PWFB are lightweight and easy to be transported and moved. Once an array of road barriers is assembled, they are filled with water to keep them stationary. However, there are no standards or recommended level of water inside PWFB. Existing water-filled road barriers weigh less than 70 kg when empty and can be filled up to 600 kg of water [1, 2].With water inside the barriers, PWFB has the potential to display good crash attenuation characteristics at low to moderate impact speeds.

Road safety barriers need to undergo strict governmental testing before they are allowed to be used on roadways. With recent changes in the road safety standards [3, 4], current barriers may not conform to these new sets of requirements. Full scale vehicle-barrier tests are very costly (up to $25,000 a test) [5] and only the impact reaction of the barriers and vehicles are obtained as outputs of normal tests. Hence, researchers and road barrier designers opted to utilise numerical simulations at design stages prior to testing involving actual vehicles.

Finite Element Analysis (FEA) is widely used in the scientific community due to its low cost and tremendous benefit which enable researchers and designers to make better design decisions. Most research regarding road safety barriers involves barrier with homogenous material properties such as concrete barriers [6-8] and steel barriers [9-11]. Modelling a PWFB system presents a challenge due to the fact that the flexible, plastic barrier model involves solid and fluid sections. Jiang et al.[12, 13] used multi-body system to model the impact response of a 30m length PWFB system via MADYMO. However, the sloshing effects of water were not accurately documented nor visualized in the model due to fluid being assumed as a solid rigid body in the hollow container. From Jiang's model, it is evident that FEA is efficient at solving high speed impact problems to analyse PWFB. However, the rapid fluid motion created by water poses a challenge in elemental discretisation and contact modelling due to complexities caused as the problem size increase. This outlines the need for further studies to explore more effective numerical models to treat this problem.

In recent years, to overcome the shortcomings of the FEM, a group of meshless methods has been proposed. In addition, the coupling method between the mesh-less methods and FEA has also been developed to take full advantages of both methods[14, 15].Smoothed Particles Hydrodynamics (SPH) is a meshless computational Lagrangian hydrodynamic particle method. This method originated approximately 40 years ago when it was used to model astrophysical phenomena without boundaries [16, 17]. It has been used in many fields of research including astrophysics, ballistics, solid mechanics and oceanography [18-21]. Furthermore, SPH is a suitable alternative to FEA for the study of the dynamics of a continuum under large distortions particularly in Hyper-Velocity Impact and Magneto Hydro Dynamic problems [22, 23].

SPH is based on interpolation theory by utilising kernel approximation and particles approximation respectively. The conservation laws of continuum dynamics in the form of partial differential equations are transformed into integral equations through the use of an interpolation function for kernel estimation. This method of modelling makes use of particles as the frame for interpolation and as carriers of material properties i.e. mass, density, constitutive laws. The particles are not directly connected to one another but rely on the smoothing length to "smooth" their properties by a kernel function through the Conservation Laws [17]. Modern explicit analysis codes such as LS-Dyna have integrated SPH solvers formulation within its solvers with a variable value of smoothing length in line with the Conservation of Mass. The main features of SPH were extensively described by Liu [21, 24], Monaghan [25] and Benz [26].

SPH is one of the most matured forms of meshless particles method available. However, it still suffers from the implementation of sharp boundary conditions. This causes difficulty in implementing well-defined domain conditions for fluids in fluid-structure interaction. Efforts have been made to treat the fringe conditions by coupling it with FEA [27-29]. This method achieved some success [30-33] but is susceptible to particle penetrations at higher velocities due to large pressures at the interface region. Other methods to create boundary conditions such as the use of ghost particles[21] or boundary transition region technique[34-36] are available to treat the interface region of SPH/FEA but were not used in this research. The use of FEA as a boundary presents inconsistency problems at the interface region between the two methods. Another limitation that plagued the SPH method is the tensile instability of the particle model which involves a numerical collapse of the continuum under tension. Considering tensile instability particularly occurring in solid material problems, an issue –even if it exists, is not very evident for SPH pertaining to the research in this paper.

The aim of this paper is to study the fluid-structure interaction of water inside road safety barriers using coupled SPH/FEA with non-structural mass (NSM). A numerical model based on a validated model was developed and analysed under several impact parameters. To improve the computational efficiency, the model treating water as a NSM is proposed to substitute the coupled SPH/FEA method. Coupled SPH/FEA will take advantage of boundaries created by FEA elements with high distortion capability of meshless particles in order to accurately model water in PWFB application.

NSM are additional mass spread by an area weighted distribution to a given section in the model. In this option, the mass can be artificially added either via nodes or parts in the model. The input would be the desired additional mass assigned on chosen node sets or parts. NSM allows the mass of the water to be added without generating specific elements to represent the fluid; as long as fluid-structure interaction is not of major interest in the study. NSM equal to the mass of water were applied to adjacent non-impacted road barriers. The time-step of elements are not affected by the addition of NSM. Later on, the mass of water in all the road barriers were substituted with NSM. This model is defined as FEA-NSM method and impact analysis results were compared with FEA/SPH/NSM model. Computational resources were efficiently managed without the focus on fluid-structure interactions in FEA-NSM model. This technique to model the water as an applied lumped mass on deformable road barrier has not been investigated.

The errors associated with substituting water with NSM for fluid-structure interaction is determined by analysing the kinetic energy and lateral displacement of the barrier in this research. The effect of placing NSM in the barrier instead of fluid-structure interaction was observed. Then, the advantages and drawbacks of NSM with respect to computational time and the cost-benefit involved in its application are reported. By omitting coupled SPH/FEA from the model, computational efficiency can be increased. Consequently, efficient

computational usage will improve solution time involving problems with size as massive as a full scale vehicle-barrier impact model.

2. OVERVIEW OF SPH COUPLING

The SPH method is based on an interpolation technique in which any physical field f(x) to be approximated by a smoothed value $\langle f(x)\rangle$

$$f(x) = \int_{\Omega} f(\vec{x}')W(\vec{x} - \vec{x}', h)d\vec{x}' \tag{1}$$

With *f* as a function of position vector *x* defined in the domain Ω. The kernel function $W(\vec{x} - \vec{x}', h)$ is centred at point *x* and is a function of position. The range of domain where W is non-zero is controlled by the smoothing length, h. The function *W* is usually chosen to be an even function that satisfies the normalization condition, delta function property and the compact condition which are outlined in eqns. (2-4).

Normalization condition
$$\int_{\Omega} W(\vec{x} - \vec{x}', h)\mathrm{dx}' = 1 \tag{2}$$

Delta function property condition
$$\lim_{h\to 0} W(\vec{x} - \vec{x}', h) = \delta(x - x') \tag{3}$$

Compact condition
$$W(\vec{x} - \vec{x}', h) = 0 \; when \; |x - x'| > \kappa h; \tag{4}$$

κ is a constant to the smoothing function, the kernel approximation consists of integrating the multiplication of an arbitrary function and smoothing kernel function. The integral represents an approximation by summing up values of all the neighbouring particles. The most commonly used form of the kernel function is the cubic B-Spline kernel which is

$$W(R,h) = \frac{3}{2\pi h^3} \times \begin{cases} \frac{2}{3} - R^2 + \frac{1}{2}R^3, & 0 \le R < 1, \\ \frac{1}{6}(2-R)^3, & 1 \le R < 2, \\ 0, & R \ge 2 \end{cases} \tag{5}$$

$$with \; W(x - x', h) = W(R, h)$$

Thus the gradient of function *f* can be approximated by using Eqn (1) via integration of parts and the compact support of the kernel allows the surface terms to be discarded.

$$\langle \nabla f(x)\rangle = \int_{\Omega} f(\vec{x}')\nabla W(\vec{x} - \vec{x}', h)d\vec{x}' \tag{6}$$

The continuous integral is then transposed to a discrete approximation for the case where physical field is known at a set of discrete SPH particles.

$$\langle \nabla f(x)\rangle_i = \sum_{\mathrm{j}=1}^{\mathrm{N}} V_j f(\vec{x}')\nabla W(\vec{x} - \vec{x}', h), \tag{7}$$

V_j denotes the volume of given particle *j*. The particles are considered as nodes, thus each nodes represents a material. The field values of density and pressure are known at the particle which moves with the material. This allows a set of particles within the support particle *i* to change enabling large deformation to be visualized

without issues. Then, applying the process to the momentum equation of continuum mechanics allows the SPH derivation of the momentum equation.

$$\frac{dv_i}{dt} = -\sum_j m_j \left[\frac{P_i}{\rho_i^2} + \frac{P_j}{\rho_j^2}\right] \Delta_i W_{ij} \tag{8}$$

Where P_i and ρ_i are the pressure and density respectively of particle *i* and P_j and ρ_j are the pressure and density of the particle considered at *j*. The application of common SPH form of the momentum equation causes the boundaries to be difficult to define. This is because each particle is its own centre of sub-domain with radius *2h* which causes the boundary to diffuse over this length. To circumvent the need to create a surface geometry using SPH particles, a contact potential, $\varphi_x$based on the kernel function is used [29]. The function is defined as

$$\varphi_x(x_i) = \int_{\Omega_c} K \left(\frac{W(x_i - x_j, h)}{W(h_{avg})}\right)^n \mathrm{d}V \tag{9}$$

x_i and x_j are the coordinates of two particles in different bodies, h_{avg} is the average value of *h* of the two considered particles. *K* and *n* are user defined parameters which control the shape and magnitude of the potential. The discrete form of this contact potential is derived and used to define the contact force, f_c:

$$f_c(x_i) = \frac{m_i}{\rho_i} \sum_j \frac{m_j}{\rho_j} Kn \left(\frac{W(x_i - x_j, h)}{W(h_{avg})^n}\right)^{n-1} \nabla \mathrm{W}(x_i - x_j, h) \tag{10}$$

The addition of these force vectors is sufficient to the contribution of the internal and external force in the momentum equations of the FEA and SPH solvers [29]. The contact force is applied between SPH particle and FEA nodes which lies within 2*h* of considered particle [29].

3. MODEL OF ROAD SAFETY BARRIER

The numerical model was developed using the commercially available software MSc Patran™ and solved in LS-Dyna3D©. A model of three plastic road barriers, aligned together is generated for SPH/FEA full modelling. The SPH particles for filled water are located inside a hollow road safety barrier modelled using shell elements as depicted in Figure 1(ii). Different height of water can be obtained by specifying (relative to the volume of shell enclosure) the percentage fill level during the particle generation phase. Overall, the model consisted of shell elements, solid elements and SPH particles.

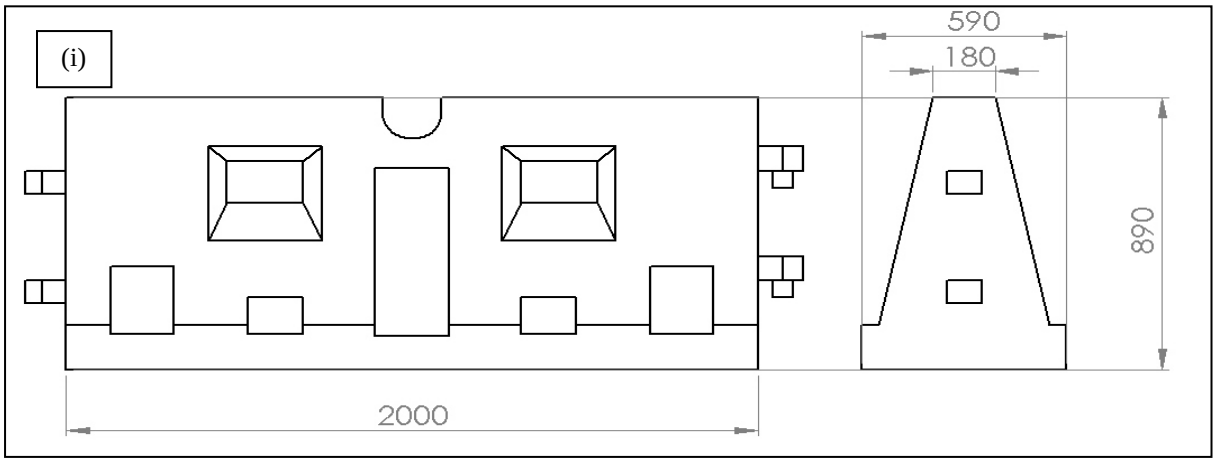

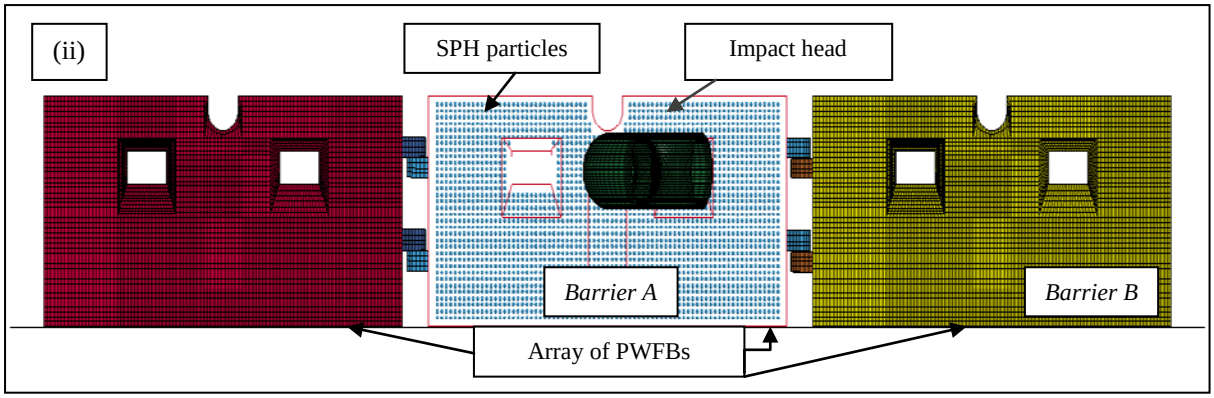

Figure 1: (i) CAD Model of Centurion 2M PWFB; (ii) FE Model of Centurion 2M barriers

This research worked closely with the industry to improve road barrier products. The model of the barrier was modelled after Centurion 2M Zone Barrier [37] as shown in Figure 1(i). The road barrier was manufactured by rotational-moulding process of Medium Density Polyethylene (MDPE). In general the barrier has a rectangular base with 145mm height. The main body has a slanted 12° angle onwards as per designed by the manufacturer for ease of storage. The variations caused by manufacturing yields an average thickness of 5mm. The barrier's overall dimensions were: 2000mm (L), 890mm (H), and 590mm (W). Retailers of Centurion 2M claimed that it suited the criteria of NCHRP 350 TL-1 [38]. Though it can be filled up to 600kg of water, recommended water level is only up to 225kg [37]. The model of the barrier system consisted of three assembled barriers in a row which is generated using 47,581 shell elements with 20mm edge. Each road barrier consists of two separate parts (main body & joint mechanism). The main body is the central section of the barrier which is subjected to impact. In addition, the joint mechanism connects the barrier to adjacent ones. Detailed FE modelling of the joint mechanism was carried out to connect the barriers. Similar to the real world, the joints consist of two female-male joints at each end which fastened to adjacent joint. The male joint is 60mm in diameter with height of 60mm. The female joints consist of 80mm diameter hole with a 75mm depth. This gives a 10mm gap between the joints after assembly. Furthermore, the addition of joints causes the main body of barriers 150mm separation between the main bodies of adjacent barriers. The gap causes delayed response of the PWFB as a system. The original geometry of the barrier was further simplified in order to build a regular mesh that allowed focus on the interaction between structure and the fluid inside the tank. Small grooves and edges that exist on the surface of the barrier were not modelled to simplify the model. These grooves were placed to avoid long continuous section on the barrier which contributed to unwanted warping during cooling after fabrication of the barrier hence it was not modelled.

The Belytschko-Tsay [39] single integration-point shell formulation was used with volume and stiffness based hourglass control element formulation. The material model of Gover [32] based on recommendation of Lobo [40] and LS-Dyna [41] was applied in this study. This element model is suitable to model materials that exhibit indistinguishable elastic-plastic regions. It is used to handle complex behaviour of ductile-brittle transitions where failure strains can vary anywhere between 100% and 10% depending on the polymers [40]. The material model, known in LS-Dyna as *MAT_89* follows closely the formulation of the commonly used *MAT_24* model in the treatment of plasticity. *MAT_24* divides the response of material into linear and non-linear components. The linear response follows a linear relationship defined by a specified Young's Modulus and limited by the yield stress. Once an element goes over the set yield stress point, the material behaviour enters the elastic-plastic region. This region is governed either by the Cowper-Symonds yield scaling method or a definition of true-stress-strain plots over multiple strain rates. Element failure is achieved via the specification of plastic strain for material failure.

Unlike *MAT_24*, *MAT_89* enables the specification of entire true stress-true strain profile rather than breaking up the data into elastic and plastic regions. This ensures that the initial non-linear elastic response of the polymer is simulated. Elastic or plastic deformation is determined in the model based on the local modulus of the specified stress-strain data. The slope of the curve is internally checked by LS-Dyna. The model is considered to have yielded if the tangent slope is less than the specified Young's modulus. In the elastic-plastic region, the

yield stress vs. strain rates was used to model the rate-dependency rather than the Cowper-Symonds equations. Scaling of the stress-strain curve was more beneficial as it allows the model to be applied at higher strain rates.

Implementation of this element model is specific to the PWFB. Specimens were obtained from various locations of a dismantled PWFB. Laboratory tensile test of samples at rates of 20, 200 and 500 mm/min were conducted in accordance with ASTM D638 Standards [42]. True-stress vs. true strain relationship of the material was formulated from the tensile test. Then, the true-stress vs. true strain curve for MDPE (Figure 2) and the yield stress-strain rate dependency (Figure 3) were exported to *MAT_89* in LS-Dyna. Furthermore, Gover reported that the material model exhibited erratic and unstable behaviour at the onset of plasticity in the model. He attributed it to the nature of explicit FEM where high frequency resulted from small variation at the node. However, Gover judged that these oscillations have little effect on the response of element during impact simulations. Thus, a simple low-pass filter option was available and successfully employed to treat high frequency oscillations from the strain rates prior to their use in rate effect calculations. The material properties of MDPE are outlined in Table 1.

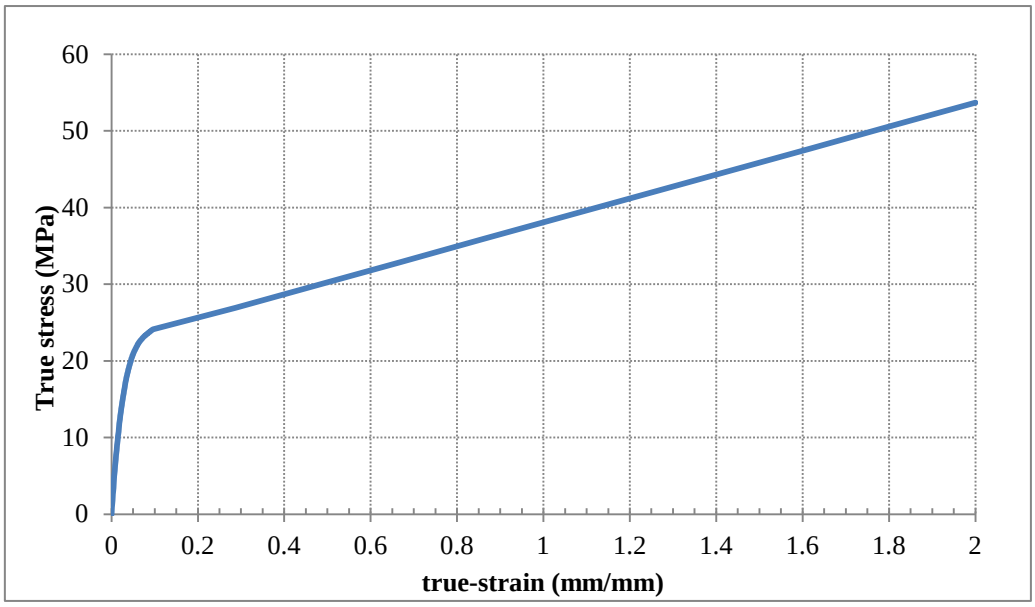

Figure 2: True-stress vs. true strain of MDPE

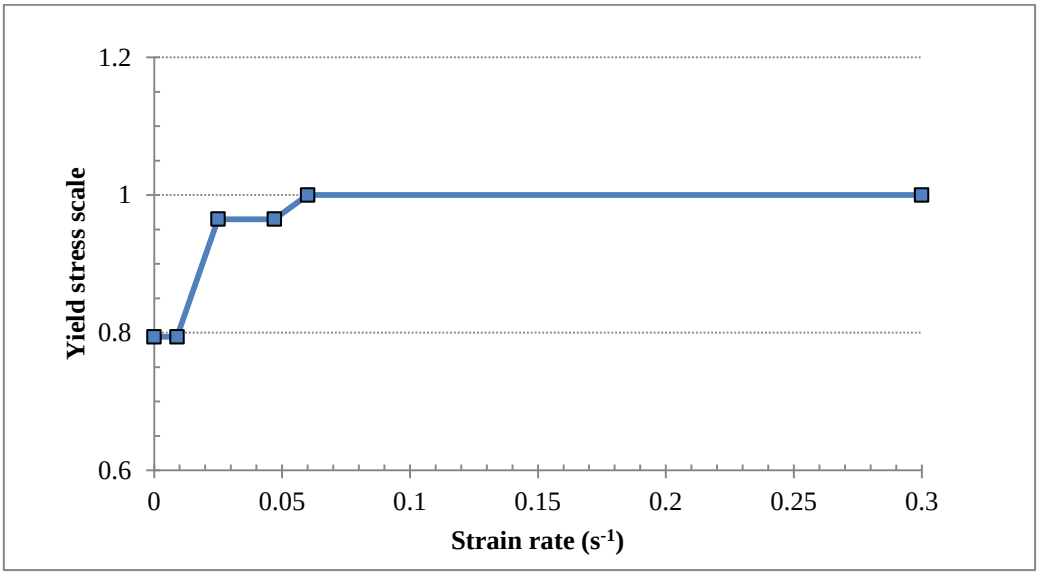

Figure 3: scale of yield stress over strain rate

Table 1: Properties of MDPE

Material	Density (kgm^{-3})	Poisson Ratio	Yield Stress (MPa)	Young's Modulus (MPa)
MDPE	948.0	0.40	10.8	312.0

The impact head used in the experiment was modelled as a rigid impact head. The head replicates the front bumper of a car with a height of 400mm relative to the ground. Rigid material properties were assigned to the head with 300kg mass. The impact of the head was set at 25° angle in conjunction with the impact parameter outlined in current standards for safety structure evaluations [43].

Joining mechanism of the barriers was achieved by pin-hole connecter similar to real PWFB. The pin-joint section was fixed to the main body by tying overlapping nodes of the joining parts onto a common surface. Tying intersecting nodes ensures the two parts remained attached. Contacts at the surface joints between road barriers follow the standard penalty methods in explicit program codes which are the most generally used interface algorithms. This contact method places normal interface springs between all penetrating nodes and the contact surface. The algorithm applies an interface force between slave nodes and their contact point whenever penetration is detected. The surfaces between the joints of adjacent barriers are smooth (polymer to polymer) hence friction between them was negligible. Besides that, contacts between the ground and the road barriers shared the same contact formulation as earlier discussed but friction coefficient between the ground and the barriers was set to 0.3; based on the findings of Shane [44].

3.1 Interface of the Coupled SPH/FEA for Fluid-Structure Interaction

The relative ease to generate SPH/FEA full model is possible because SPH formulation is integrated in LS-Dyna solver. The application of SPH/FEA full model in road safety barriers presents several advantages as well as drawbacks. The stability of SPH/FEA full model featured in road safety barriers is dependent on the impact speeds and number of particles being used in the model. Generating SPH particles by volume fill enable particles to be generated onto complex geometrical structures such as water-filled barriers. However, the need to specify arbitrary gap between the interacting elements and particles causes irregular placement of particles due to the initial gap that is not the same as the specified distance of particles in all axial direction. On the other hand, the construction of solid elements to fill the hollow body as a medium to create SPH particles is a more efficient option. This creates a genuinely consistent length between each particles as well as consistent distance between particles and FEA elements. This method of SPH particle generation was used by Anghileri et al. [30] to study helicopter fuel tank impact with the ground.

The rather complex geometrical design of the Centurion Zone Barrier means that FE model is produced prior to SPH particles generation in this study. Afterwards, the particles were generated by filling the hollow volumetric section of the FE model. SPH particle generation creates free surface for two-phase interacting fluids directly because particles represent water and empty space represents the air inside the hollow container. Generated elements are used efficiently in the system and rapid water sloshing is visualized in the model. An arbitrary gap between SPH and the membrane has to be specified to avoid initial interpenetrations during solution. Interpenetration occurs when the slave nodes i.e. SPH particle is detected to be too near to or overlapped the length of projection vector of the membrane shell thickness. The farther the distance between SPH particles and the FEA elements, the more stable the calculation of SPH/FEA will be. This in turn reduces the probability of SPH particles going outside of the specified boundary set by the FE mesh. However, a large gap at the interface leaves a significant lag response of the water to the impact which delays the energy transfer between the shell elements and SPH particles inside the enclosure. The tolerance distance for penetration distance can be altered to ignore initial interpenetrations but the default value is used in this analysis. The authors found that the minimum gap that can be allowed is one half of the shell element thickness [45]. This confirms findings from Campbell et.al. [27] [46]with regards to the distance between the elements and particles in coupling.

During impact, water interacts with the solid structure of the barrier's membrane. Fluid-structure interaction is defined by the penalty method algorithm with soft constraint penalty formulation. The contact is somewhat

similar to contact defined between adjoining barriers but additional treatment is required as it involves two materials with largely different stiffness values. Soft material such as water lowers the stiffness values in the slave nodes causing disproportionate penetrations in the model. SPH particles are considered slave nodes interacting with the surface nodes of the FE mesh. Therefore, in addition to the master and slave contact stiffness, an extra stiffness value according to Courant's criterion is calculated based on the stability of the local system of two masses connected by a spring [47]. The stability contact stiffness k_{cs} as function of time is defined as:

$$k_{cs}(t) = 0.5 \cdot SF \cdot m^* \cdot \left(\frac{1}{\Delta t_c(t)}\right) \quad \textbf{(11)}$$

SF is the scale factor for the Soft Constraint Penalty Formulation and set to the default value (0.1), m^* is a function of the mass of the slave node and the master nodes computed internally by LS-Dyna solver. Δt_c is set to the initial solution time-step. If the solution time-step increases, unstable behaviour is averted by resetting Δt_c to the current time-step. Interaction between water and shell of the barrier occurs throughout the barriers segments. However, modelling water inside each barrier can be computationally exhaustive. Maximum sloshing is inferred inside the main impacted barrier while the adjacent barrier provides inertial resistance. Therefore, SPH particles were generated only in the centre barrier.

3.2 Fluid Formulation of Water

Fluid section of the barrier comprises of SPH particles. The large distortions due to rapid sloshing are unable to be obtained using FEA alone. Thus, particles were introduced as a fluid domain to visualize mesh deformations. The Navier-Stokes equation is the foundation to fluid mechanics. To model water, the Navier-Stokes theorem governing the general hydrodynamics is employed through SPH formulation encoded within LS-Dyna. Fluid particle approximation with normalization formulation was chosen as the particle approximation formulation because water is represent by the particles.

Under the conditions of impact, the sloshing of water can be deemed incompressible. The SPH solver used assumes that all materials are compressible hence bulk stiffness is defined by an Equation of State (EOS). The use of EOS was invoked to describe the properties of water in the road barrier. Because water is a commonly used fluid, the constants in the EOS for water are widely available in the literature [21, 48]. The Mie-Grunesien equation of state for fluid pressure takes the form of Equation (12) during compression and Equation (13) during expansion i.e

$$p = \frac{\rho_0 C^2 \mu \left[1 + \left(1 - \frac{\gamma_0}{2}\right)\mu - \frac{\alpha}{2}\mu^2\right]}{\left[1 - (S_1 - 1)\mu - S_2 \frac{\mu^2}{\mu + 1} - S_3 \frac{\mu^3}{(\mu + 1)^2}\right]} + (\gamma_0 + \alpha\mu)E \quad \textbf{(12)}$$

$$p = \rho_0 C^2 \mu + (\gamma_0 + \alpha\mu)E \quad \textbf{(13)}$$

The Mie-Grunesien EOS models the water as a compressible fluid by using cubic shock velocity and fluid particle velocity to determine the pressure of compressed and expanded water. In both equations (12) and (13) above, μ is defined as (η-1) where η is the ratio of the densities before and after the impact, ρ_0 is the material density, C is the bulk speed of sound, γ_0 is the Grunesien gamma coefficient at the reference state, α is the first order of volume correction to γ_0. S_1, S_2, S_3 are the coefficient slopes in a linear Hugoniot line of the shock wave velocity slope and E is the internal energy per unit volume. The Mie-Grunesien EOS option in LS DYNA was used to input C, S_1, S_2, S_3, γ_0, α which are user defined parameters. In the initial setup of the simulations, the density was added in particle generation and material properties section while the remainder were input in the EOS section of LS-Prepost. The parameters for the EOS were taken from Steinberg's [49] experimental data and are listed in Table 2.

Table 2: Material parameters and coefficients in the EOS for water

Symbol	Meaning	Value
ρ_0	Initial density	1000 kg/m^3
C	Speed of sound	1480 m/s^2
γ_0	Grunesien gamma coefficient	0.5
α	Volume correction coefficient	0
S_1	Fitting coefficient	2.56
S_2	Fitting coefficient	1.986
S_3	Fitting coefficient	1.2268

To study the different parameters that affect contact at the interface of SPH and FEM, parametric impact simulations were done with several varied parameters. Figure 4 describes the interface at the boundary of SPH/FEA full model. Three particle nodes and three shell elements are depicted in Figure 4. Each particle represents the volumetric spatial area it incorporates.

Firstly, the shell mesh thickness was varied to see the effect it has on the contact response of the barrier subject to impact. The thickness values were decreased from its initial thickness without specifying any distance between particles and elements. Varying the thickness affects the projected contact surface at the boundary. Secondly, the space on the interface of the SPH/FEA full model region was varied to determine the effect of size of space in relation to contact consistency. The initial distance between particles and meshed elements was varied by setting a specific distance during the SPH particles generation phase.

The barrier fill level was set constant at 50%. With initial particle distance of 25mm between particles, it takes 27,124 particles to half-fill the barrier with water. The impact head had an initial velocity of 8ms^{-1} in a single direction of impact. The penetration occurrences and calculation duration of the SPH particles at different clearance gaps and shell thicknesses were extracted.

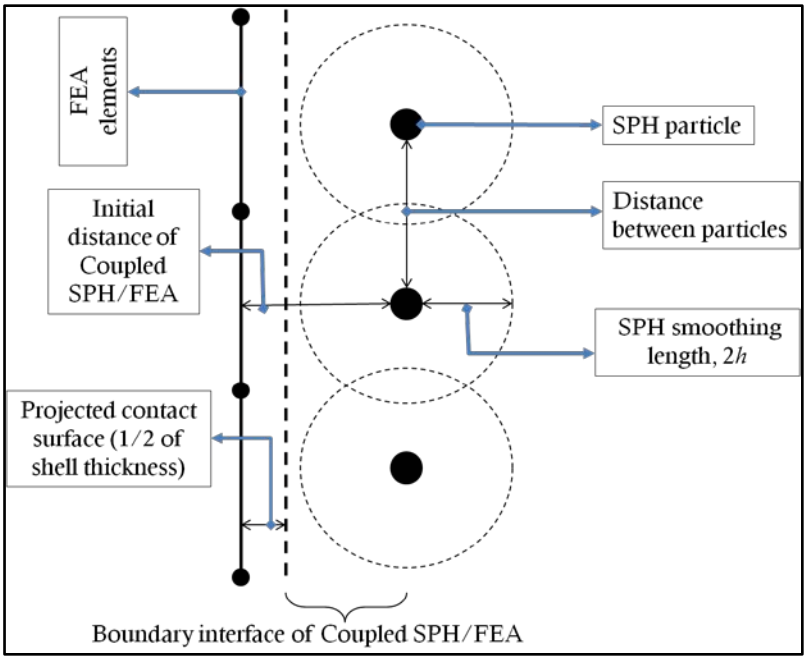

Figure 4: Interface region of coupled SPH/FEA

Varying the shell thickness causes contact failure to occur. This is evident when the number of particles penetrating the barrier increased with thinner membrane thickness. This is attributed to the stiffness of the shell that causes the disproportionate penetrations in the model. Varying the thickness changes the boundary vector of

the projected contact surface in the region. The coupling of both methods depends on the ability of particles and elements to 'detect' each other during computation. This factor relies on the projected contact surface and the smoothing length. A particle will only detect boundary nodes which fall within its sphere of influence set by the smoothing length. On the other hand, changing the spatial gap at the boundary leads to stable results during initial stages of impact. Less penetration is reported because the spatial gap between FEA elements and SPH particles is wide enough for stable calculation. However, a large enough gap will leave a lag in energy transmission at the boundary. This is due to the fact that the elements will need to traverse additional space before interacting with SPH particles. Slower response in SPH/FEA full model means more energy will be absorbed by the meshed elements leading to elevated levels of recorded stress in FEA. Overall, the interface region is a very important section in fluid structure interaction. The boundary region is susceptible to inconsistent penetration occurrences. Various treatments to counter the penetrations are available such as lower time-step, bulk viscosity and dynamic relaxation of the model but at the compromise of longer computation duration.

3.3 FE Model Validation & Comparison

The best approach in the study of numerical simulation is to validate the model with results from laboratory experiments. In early 2013, at *QUT Banyo Pilot Plant Precinct* (PPP) of *Queensland University of Technology*, an intensive program to test plastic road safety barrier was performed. One of such test involves the impact of PWFB by a horizontal impact head. The road barriers were impacted with $6ms^{-1}$ velocity at 55°. Water was filled to 200kg. *Barrier A* and *Barrier B* shown in Figure 1(ii) was designated for validation of the FE model. *Barrier A* denotes the centre barrier which was impacted. Next, *Barrier B* represents the upstream barrier adjacent to the impacted *Barrier A*. The event was captured by a high speed camera fixed overlooking the impact 100cm atop of the region of interest. No failure of the shell was observed during testing. Subsequently, video analysis was use to obtain the lateral displacement-time relationship of the road barriers. The lateral displacement of respective road barriers was plotted by determining the location of an arbitrary point-of-interest on the road barrier at each time frame across the entire captured sequence of the event.

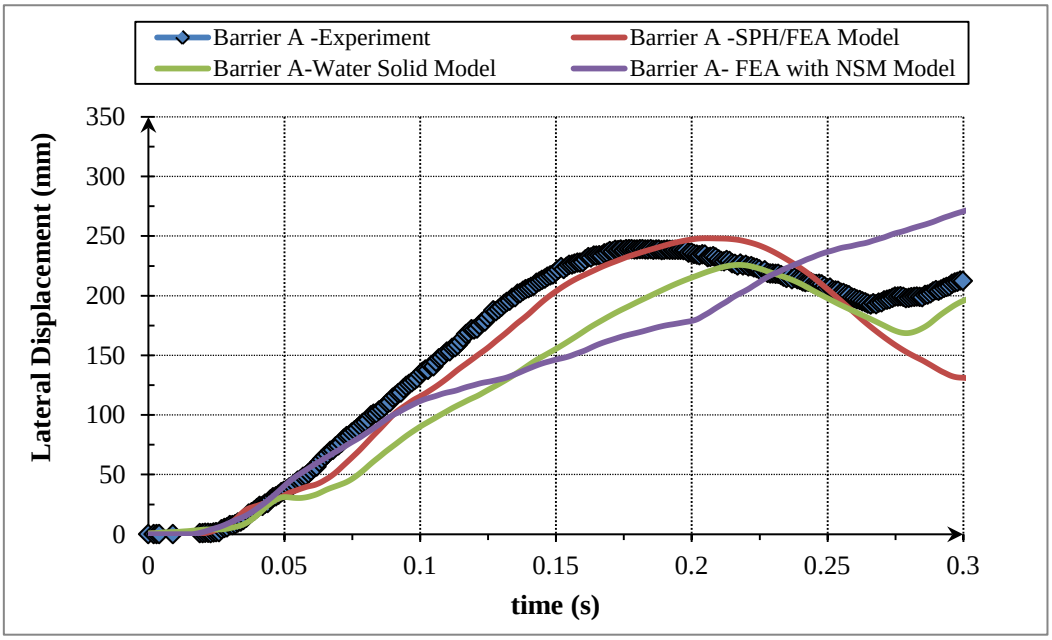

Figure 5: Comparison of lateral displacement of validated impact model of *Barrier A*

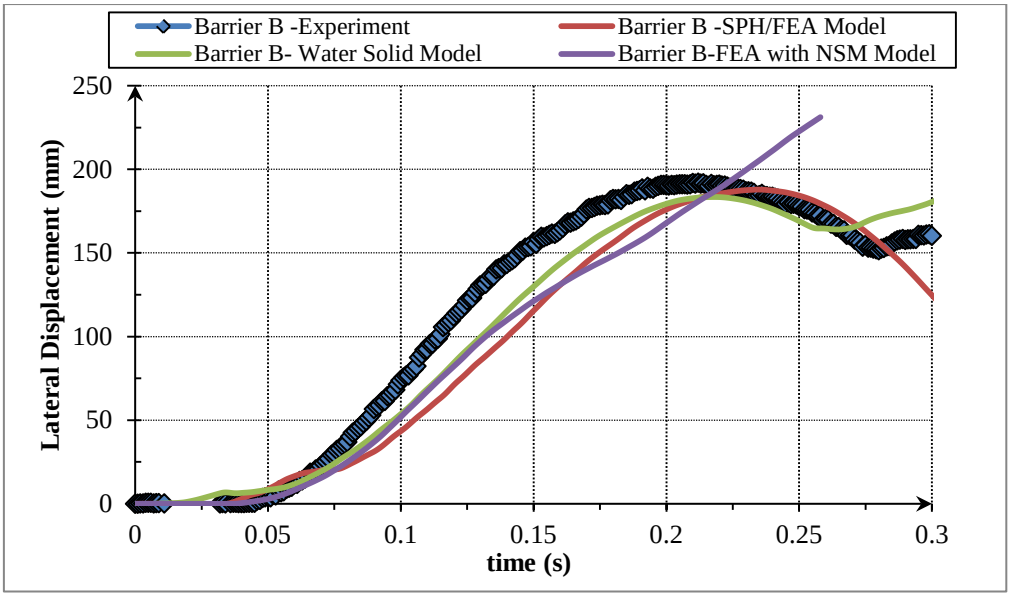

Figure 6: Comparison of lateral displacement of validated impact model of *Barrier B*

Three methods to model water in the road barriers were probed. They were i) SPH/FEA full model ii) Solid water model and iii) FEA-NSM model. All the models were executed under similar impact parameters as the experiments. The lateral displacement of *Barrier A* and *Barrier B* from each model were compared against obtained experimental results. The lateral displacement-time relationship of *Barrier A* and *Barrier B* are shown in Figure 5 and Figure 6. It can be seen that the SPH/FEA full model yields the best correlation with experimental results in both barriers. On the other hand, the least similar result is the FEA-NSM model which severely underestimates and overestimates the displacements of the model. The only benefit the FEA-NSM has over its counterparts is faster solution time. This severe discrepancy is expected due to the simplification of the model water as lumped distributed mass. The water as a solid model provides a viable option to treat water however the effect of sloshing was unable to be visualized due to water being confined to gridded elements.

4. TREATMENT OF MASS BY TWO DIFFERENT MODELS

The mass of a road barrier consist of mass of the plastic shell and water which it contains. A single unit of plastic road safety barrier can vary its weight anywhere between 30kg to 600kg. The coupled SPH/FEA model was optimized to become FEA/SPH/NSM model. This model was defined as coupled analysis utilizing SPH particles alongside traditional FEA combined with NSM. This FEA/SPH/NSM model has a unique advantage that it only uses full SPH for the barrier under the direct impact and uses NSM for other barriers. Therefore, this model can significantly save computational cost while still keeping simulation accuracy. The objective of modelling water with FEA/SPH/NSM model is for fluid-structure interaction between the shell walls and water only at the impacted barrier. However, it was unclear whether it is beneficial to model water inside the barrier with respect to energy absorption if water is not the major focus of the study. Meanwhile, FEA-NSM model applies the mass of the water using NSM in all three road barriers. Water absorbs crash energy through sloshing action and inertial displacements. Modelling the barrier using FEA-NSM will only consider the inertial effects of water.

A set of barriers with a range of fill levels using the FEA/SPH/NSM model were impacted with several impact velocities. The angle of impact was assigned to 25° relative to the barrier. Then, the simulations were repeated by FEA-NSM as water under similar input parameters. The energies dissipated by water from sloshing and inertial effects were able to be distinguished. The computational time and kinetic energy of the shell were taken as output parameters. Afterwards, the model was expanded to a larger scale and with an actual vehicle model.

4.1 Response of Road Barrier under Impact

The objective of the simulation was to determine the errors involved between the two applied methods to treat water. Different fill levels at high speeds were use to extend the findings based on the validated model. The final lateral displacement and energy balance of the model were taken as output comparison. In the simulations, response of the barriers from 0s to 0.32s was recorded. The impact head was given a specific velocity-time relation. The velocity profile allowed the impact head to penetrate the road barrier over 30ms^{-1} duration at varying velocities. Then, the impact head was artificially stopped. The specific velocity-time profile was preset to prevent additional impacts after the first initial contact between the impact head and the assembled road barriers. Multiple impacts may add additional energy other than the initial instance of impact. The kinetic energy and lateral displacement distance of the centre road barrier were extracted for analysis. Figure 7 shows the head impacting the barrier in FEA/SPH/NSM model. Sloshing can be observed in the centre barrier when the impact head collide with the assembled PWFB.

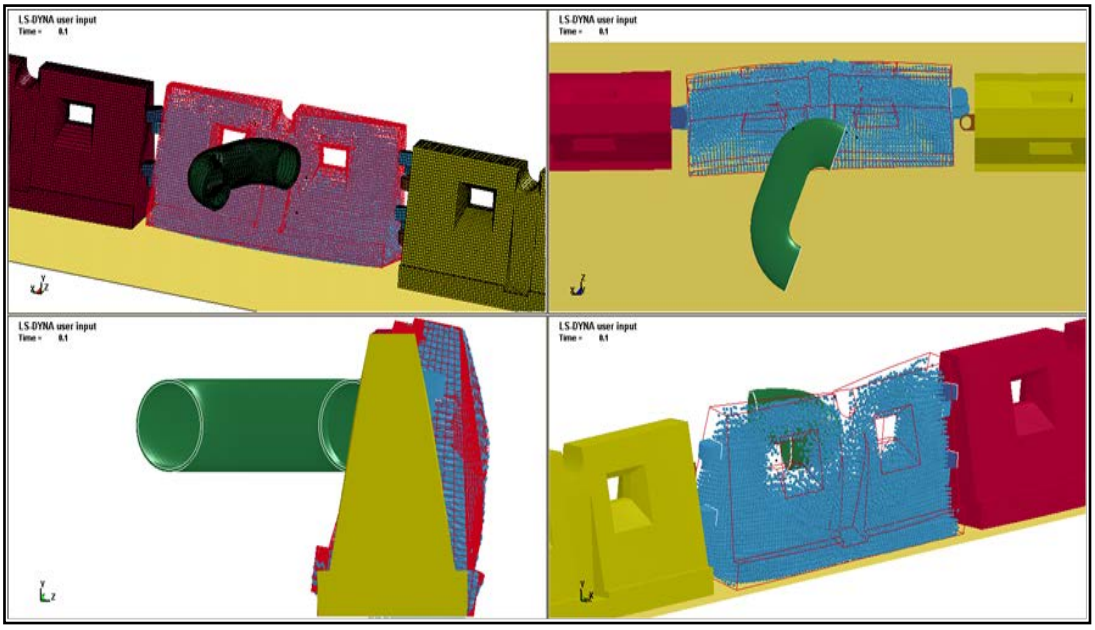

Figure 7: SPH/FEA interaction in FEA/SPH/NSM model of barrier impact at 80kmh-1 at 100% fill capacity

Figure 7 depicts the impact of a row of three road safety barriers by the rigid body at 25° with a velocity of 80kmh^{-1}. The computational time of each simulation case by both FEA/SPH/NSM and FEA-NSM model were tabulated. The amount of time each simulation allowed to run was set at 12 hours using 3 CPUs; this means the solution could be run up to 36 computational hours. For all other fill levels, the models were unable to solve within the specified time. It is inferred that the computation would take longer than 36 hours to complete. The increase in simulation time is related to the computation of SPH particles compared to other factors such as impact velocities or impact angles. The computational requirement of SPH to renormalize each particle in each time-step increases the computation duration of the model. The use of more CPUs can decrease the computational duration in the model. But this requires additional computational resources for the simulation. Furthermore, the introduction of multi-processor control cuts down the solution time. The multi-processor control allows the equal distribution of SPH calculation in the model by LS-DYNA when multiple CPUs are called upon to solve the numerical model.

FEA-NSM solved faster than FEA/SPH/NSM model in PWFB. The use of FEA-NSM model to replicate FEA/SPH/NSM model can decrease the computation duration. This justifies the option of modelling water inside of the barrier with FEA-NSM. In road safety barrier, the mass of water has the ability to absorb the energy through sloshing and inertial displacements. The use of FEA-NSM was intended to influence the displacement accounted by the water mass in the barrier and disregard the effect of water sloshing. The energy from the impact was distributed to the deformation of the MDPE shell membrane, sloshing of water, and movement of the road safety barriers. The kinetic energy corresponds to the movement of road safety barriers

and sloshing of water. On the other hand, the internal energy includes the elastic strain energy and work done for permanent deformation occurred in the shell membrane of PWFB. Kinetic energies of road barriers adjacent to the impacted one were minimal compared to energy on the central barrier hence were not reported.

Deeper energy analysis was conducted on the FEA/SPH/NSM model. The graph plotted on Figure 8 shows the maximum kinetic energy of water over the range of tested impact velocity. It was found that the energy absorbed by water was related to the impact velocity. The sloshing of water in road safety barriers contributed very little in absorbing energy at low speeds (less than 50kmh^{-1}). At low speeds, the kinetic energy exhibited by water was minimal for all tested fill level. Thus, 50% fill is adequate for impact speeds 50kmh^{-1} and lower. However, water does contribute to energy absorption at higher speeds. At speeds between 50kmh^{-1} -80kmh^{-1}, the energy absorb by water are similar for fill level 80%-100%. Hence, water could be optimized at 80% fill capacity for efficient usage. On the other hand, additional water is preferred for impact velocity of 100kmh^{-1} for maximum energy absorption by water. Hence, 100% water fill level is recommended for high velocity impact of 100kmh^{-1}.

The impact location was also another aspect which determines the effectiveness of energy absorption. The point of impact is located 600mm relative to the ground. This equates to 66.7% of the road safety barrier's height. It was observed that for effective energy absorption by water inside the container, the free surface of water must be higher than the impact location. This is evident from Figure 8 which shows higher energy absorption for fill levels which were higher than the height of the impact head.

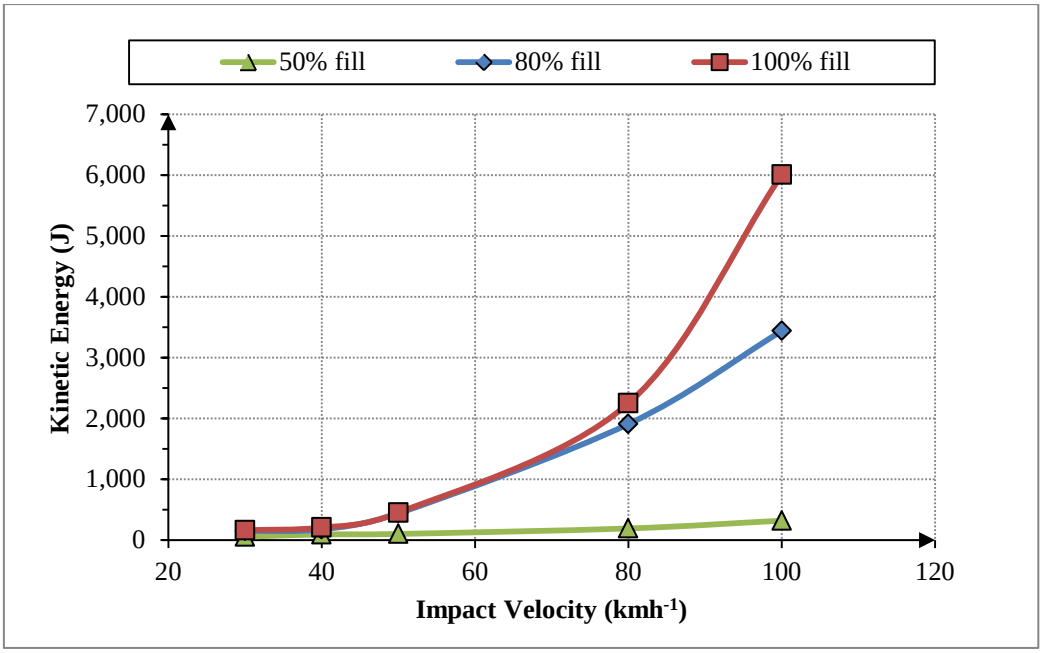

Figure 8: Maximum energy absorbed by water over range of impact speeds

$$\mathrm{ASI} = \frac{1}{2}\mathrm{m}(\mathrm{v}\sin\theta)^2 \qquad \textbf{(14)}$$

The impact of the barriers at 80kmh^{-1} and 80% filled was chosen as example of optimal energy absorption by water. The summary of total energy absorption by the *Barrier A* is plotted in Figure 9. From Figure 9, the kinetic energy of water absorbed the most energy from impact. The Accident Severity Index (ASI) [50] as outlined in Equation 14 is the lateral kinetic energy from the impact, where *m is the mass of the impacter*, *v* is the velocity of impact and θ is the angle of impact. Furthermore, the kinetic energy in the *Barrier A* was lower compared to the energy required to deform the MDPE shell of said barrier. Therefore, the probability of shell membrane failure was definite. Based on the ASI with 300 kg impact head at 80kmh^{-1}, the lateral kinetic energy the road barrier system needs to dissipate is approximately 13.2kJ. The contribution of water to dissipate energy from impact accounts for 15.1% of the overall kinetic energy dissipation. It must be noted that the percentage of

energy absorbed by water diminishes if the mass of the impacter was increased to the mass of an actual vehicle. Hence, the minimal contribution of water to dissipate energy means other prudent methods to encourage redirection is needed in the structure of PWFB. Energy absorbing materials such as steel skeleton can be augmented to the PWFB outer membrane shell of the barriers for added strength. Nonetheless, while water lacks superior crash energy absorption capability in the system, it does provide resistance to motion that enable other energy absorption materials absorb energy [51]. Due to the nature of PWFB being a temporary roadside structure, no road barriers are fully fixed to the ground. Thus, resistance to motion displacement allows additional energy absorption by other materials prior to displacement of the PWFB system.

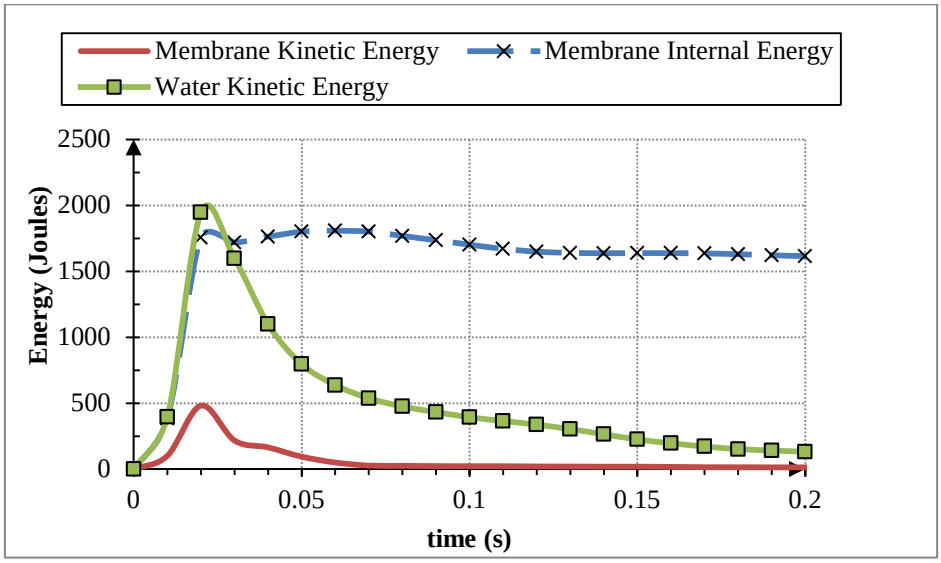

Figure 9: Distribution of energy from impact for 80% filled capacity at 80kmh^{-1}

4.2 Estimation of Errors in Non-Structural Mass Application

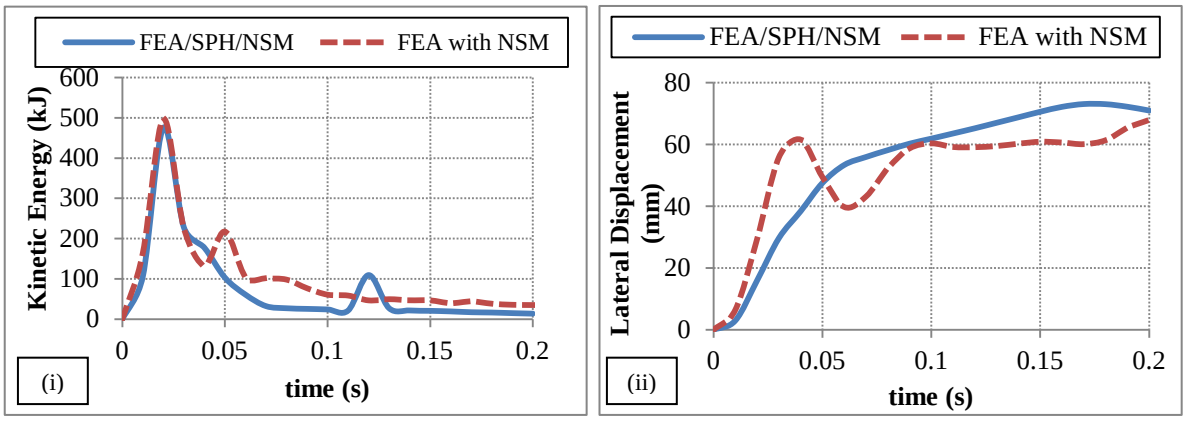

Figure 10 (i) Kinetic energy of shell membrane in both models tested; (ii) the lateral displacement of both models for impact of 80% filled at 80kmh^{-1}

Figure 10(i) depicts the kinetic energy of the shell membrane of the impacted road barrier. The maximum kinetic energy for both models was notably similar. Maximum kinetic energy occurred approximately at 0.03s when the impact head hit onto the shell membrane of the *Barrier A*. Kinetic energy of the shell membranes relates to the dissipated energy through movement of the PWFB. Furthermore, the strain energy recorded in FEA-NSM model yielded result close to FEA/SPH/NSM model. Figure 10(ii) shows the lateral displacement of the barriers after impact. Lateral displacement between both models varied all through the period of impact. Nonetheless, the lateral displacements of both models were different yet within acceptable proximity of one another throughout the computational duration. Treating water inside the barrier as a non-structural mass is an efficient way to achieve faster solution time. However, this simplification exposes the possibility of errors in the

system. The computational errors must be taken into account between the two models. For this study, the following error indicator e_{KE} , shown in Equation 15 was defined as;

$$e_{KE}(\%) = \left|\frac{KE_{full} - KE_{sph}}{KE_{sph}}\right| \text{x } 100 \qquad \textbf{(15)}$$

Where KE_{full} and KE_{sph} is the maximum kinetic energy recorded from full FEA-NSM model and the FEA/SPH/NSM model respectively. As there are no SPH particles to absorb kinetic energy in the non-structural mass model, the maximum kinetic energy exerted to the membrane shell in FEA-NSM model will always be larger than the energy in FEA/SPH/NSM model. Hence, it is inferred that $KE_{full} > KE_{sph}$ throughout this study as depicted in Figure 10(i). The two models with varied fill levels were used to simulate impact over a range of impact velocities from 30kmh^{-1} to 100kmh^{-1}. Then, using Equation (15), the error between the results of full FEA-NSM model and FEA/SPH/NSM model were obtained and plotted in Figure 11.

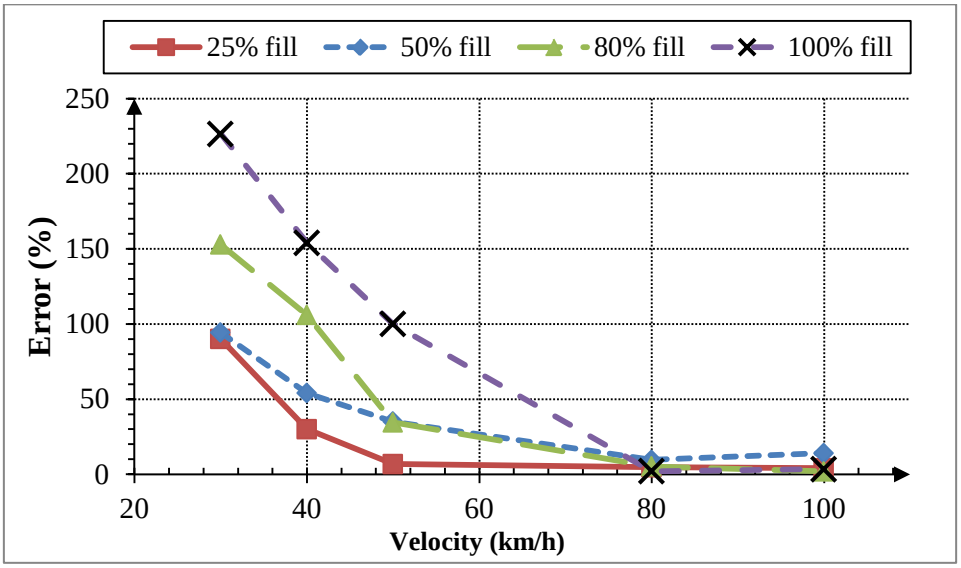

Figure 11: Velocity over the error for different fill level of the barrier

As depicted in Figure 11, bigger error is introduced to the system at low impact speeds. An impact at 30kmh^{-1} with 100% filled water shows the highest error percentage with 230% discrepancy error. Increasing the fill level would result in the increase of error for case between 30kmh^{-1} to 50kmh^{-1}. FEA/SPH/NSM model takes into account the inertial displacement and sloshing of the water in the barrier while the FEA-NSM model functions as a surrogate to water's inertial response in the road barrier while excluding energy dissipation related to sloshing. Adding more water will increase the energy absorption capacity of water in the road barrier. However, because the level of water is limited to the size of the enclosure which contains it, water in the barrier has a limit to its energy absorption capacity. Based on the error recorded, the large discrepancies can be attributed to the sloshing of water which contributes to energy dissipation at low velocities. The large water excitation in FEA/SPH/NSM model but was unavailable when FEA-NSM model were employed.

On the other hand, for cases at elevated impact speeds (80kmh^{-1} to 100kmh^{-1}), the error is relatively small i.e. between 3% to 14%. This is beneficial considering the reduction in computational-time from the simplification. The increase in impact velocity means an escalation in the energy involved in the road barrier system. Based on the Conservation of Energy, the energy in the system can be described to be the summation of all energies which consist of the energy to deform the barrier, energy to displace the barrier, energy to slosh the water and the energy remaining in the impact head. As the impact energy increases, the inertial displacement effect is more dominant than sloshing in the barrier. This can be seen when the error for all fill levels converges as impact velocity increases. In other words, the larger the error between the two models, the more evident the role of water sloshing has in the system of barriers. Thus at high speeds, the assertion that inertial displacement of water functions as the dominant energy dissipater over sloshing in PWFB is acceptable.

The above findings can also be discussed with respect to impact time. At low speeds, the impact force from the impact head to the barrier is transferred over a period of time. This allows water sloshing to be fully developed inside the barrier. Subject to the amount of water available in the barrier, energy is dissipated when fully developed sloshing is achieved. In contrast, high speeds impact involves larger impact force being applied over a shorter time period. This prevents water from reaching its full sloshing phase in time for energy dissipation. As a result, most of the energy is directed to the inertial displacement of water and the road barrier. The inertial displacement of water and barrier is reflected by the kinetic energy in the barrier.

The treatment of water by two distinct models allows the study to determine the energy being mutually yet independently dissipated by water through sloshing and lateral displacement. Moreover, the information presented in Figure 11 allows researchers to determine the suitable method to treat water inside PWFB. For example, it is advisable to use the FEA/SPH/NSM model with high water fill levels (80% to 100% fill) for better accuracy. The FEA-NSM model was unable to capture the sloshing effects which occurred during low speeds-high fill levels impact cases. However, the FEA/SPH/NSM model requires more computational cost. On the other hand, if the fill level is less than 50% fill capacity, the application of full FEA-NSM method is a viable surrogate option with acceptable errors in the analysis. Besides that, based on the intensity of the impact velocities, FEA/SPH/NSM model yields better simulation accuracy and suitable for cases with low impact velocity (less than 50kmh^{-1}). Meanwhile, FEA-NSM model is more computational efficient for velocities ranging between 80kmh^{-1} to 100kmh^{-1}. Hence, future researcher may choose the methods used to treat water in PWFB based on water fill levels and vehicle impact speeds.

5. EXTENDED FULL SCALE ROAD BARRIER SIMULATION

Based on the results obtained from the comparative analysis of impact on a set of three road safety barriers, the data presented good error to benefit ratio with respect to computational time. Further study is required to see the applicability of FEA-NSM model as a surrogate to the coupled SPH/FEA full model in a vehicle-barrier impact simulation. The FEA/SPH/NSM model was reverted back to coupled SPH/FEA model. The optimized model was reverted to see comparison of models exclusively using SPH/FEA and FEA-NSM. The comparison of the models to one another is done to determine the efficiency of each model in replicating the vehicle-barrier impact. Further optimization using FEA/SPH/NSM can be done in future once the extent of the vehicle contact with the barrier is determined.

In this section, a full vehicle impact at 80kmh^{-1} and 25° angle in accordance with the Manual of Assessing Safety Hardware (MASH 08)[43] was generated to demonstrate the performance of the coupled SPH/FEA modelling approach in PWFB. Thirteen barriers were created and placed adjacent to one another to function as a single continuous section. The longitudinal length of the set of barriers was 26 meters long with each segment of barrier being 2m in length. Each road barrier was filled with 80% water capacity equivalent to 430 kg/m in the road barrier system. Furthermore, adjacent barriers are connected with one another using simple shell plates to simulate a pin-joint mechanism. MDPE material properties of the barrier and water are assigned as previously used. For fluid-structure interaction, water particles were generated in the barrier. Subsequently, non-structural mass with equivalent water mass were assigned later in the reiterated model. Similar requirements of particle penetration treatment were needed in the extended full scale road barrier model. The simulated time displacement histories of both techniques were compared.

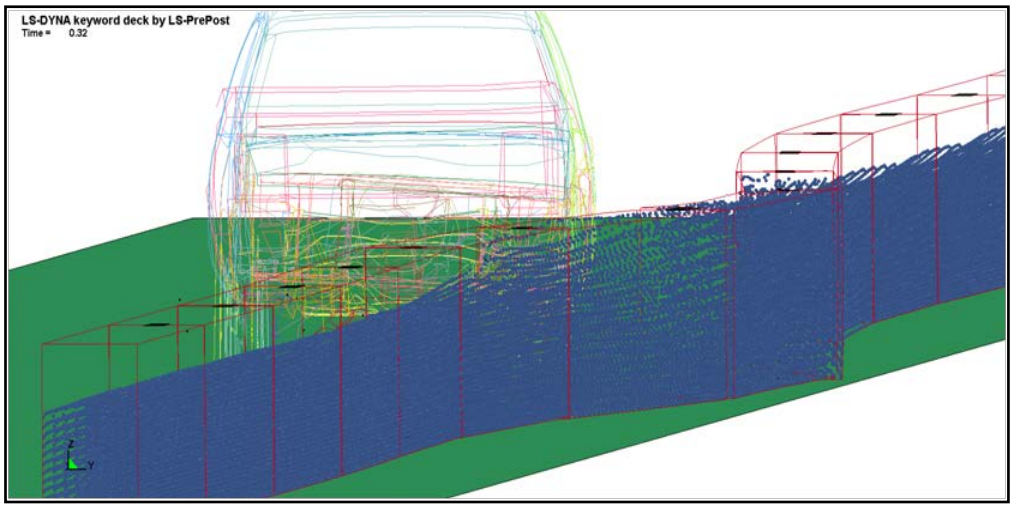

Figure 12: Water sloshing inside road safety barrier at 80 kmh^{-1}

Figure 12 illustrates the sloshing of water inside the barrier and redirection of the vehicle as required by current standards when it is impacted by the vehicle. The response of the barrier-vehicle subjected to the impact is observed to be similar for both cases. The dynamic responses of water through sloshing and splashing can be observed based on the movement of the water inside the hollow rectangular shell. For the first time, the sloshing of water inside a water-filled barrier is numerically depicted in a full scale vehicle-barrier impact model.

The graph plotted in Figure 13 depicts the displacement-time history of the farthest displaced barrier from both models in the extended full scale simulation. Although it can be argued that the response of the vehicle and the barriers are due to other factors such as the design of the barrier or stiffness of the joints, the lateral displacement of the barriers suggest that the effect is mostly attributed to the mass of the barrier. Arbitrary nodes on the barrier with the largest lateral displacement were chosen from both models and the displacements of selected nodes were plotted over time. The average error encountered between the two models is calculated to be 5.4%. This error correlates with earlier finding of the model with three barriers which had a 5.00% error for the given speed and fill level. Hence, FEA/SPH/NSM model in PWFB is a viable option to be used for full vehicle-barrier impact models when fluid-structure interaction is not a subject of major interest in the study.

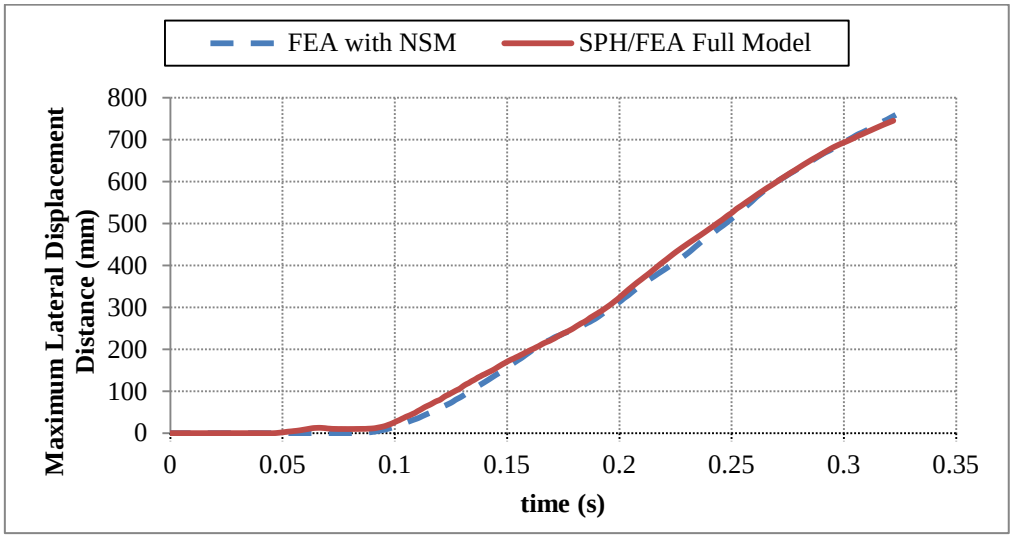

Figure 13: Displacement time histories of maximum lateral displacement of barriers

On the other hand, for those interested in the responses of the barrier under multiple parameters such as variation of fill levels, impact speeds and impact angles, treating water with full FEA-NSM model will allow an

alternative over the coupled SPH/FEA model for rapid analyses of the barriers performance under varying parameters. It is recommended that water mass be treated using a non-structural mass for velocities higher than 80kmh^{-1}. However, SPH/FEA full model is still the best method to treat water in PWFB impact and necessary for lower velocities cases for all fill levels. Alternatively, the combined model utilizing FEA/SPH/NSM model can be used to optimize SPH usage in the model. However, the extent of SPH in which barrier needs to be ascertained for a middle-of-the-road solution which inculcates accuracy and computational cost efficiency in the model.

6. CONCLUSION

Current PWFB requires water to be filled to ensure they are stationary after installation. There are no standards on the amount of water that must be filled in a barrier. The role of water in PWFB is mainly to increase the weight of the barrier and the energy absorbing capability of water in PWFB are often overlooked. There has been no work conducted to numerically visualize fluid-structure interaction in full vehicle-barrier impact simulation in order to see the benefits of filling water in the barriers. This study investigates the viability of modelling fluid-structure interaction in PWFB.

In summary, the fluid-structure interaction in PWFB where the structural response of the barrier shell is highly non-linear was modelled by full coupled SPH/FEA. This paper demonstrates that the approach can be extended to full-scale vehicle impact simulation through appropriate management of SPH/FEA at the interface region. Symptoms and treatments associated to particle penetrations in coupled analysis have been identified. Moreover, several techniques of generating SPH particles inside a hollow section were explored and discussed. Then, full FEA-NSM was invoked to replicate the water mass in the barriers to simplify the model. An optimized FEA/SPH/NSM model was employed for comparative analysis with full FEA-NSM model. The sloshing and inertial effects of water in the barrier under identical impact parameters using two different methods were presented. Findings from this research will enable future researchers to substitute SPH particles with non-structural mass for water if required. Therefore, the below conclusions can be drawn

- The use of FEA-NSM to treat water in PWFB can be a useful method if the fluid-structure interaction is not the major focus in PWFB study.
- For high impact speeds (higher than 80kmh^{-1}), inertial effects of water are more dominant than the sloshing effects of water in the barrier regardless of fill level; thus it is advisable to conduct the simulation using FEA-NSM for PWFB impact analysis at high speeds.
- At low speeds ranging between 30kmh^{-1} to 50kmh^{-1}, the effect of sloshing significantly contributes to the energy absorption of the barrier through fully developed sloshing. Hence, modelling fluid-structure interaction with SPH/FEA full model is recommended.

7. ACKNOWLEDGEMENT

This work is supported by an ARC Linkage Grant (ARC LP: 1020318). Furthermore, the authors would like to acknowledge the contribution of our industry partner, Centurion Barrier Systems Pty Ltd for their generous support and encouragement.

8. REFERENCES

[1] Energy Absorption Systems. (2010, 08/11/2010). *Triton TL-3 Barrier™ product sheet* [Webpage]. Available: http://energyabsorption.com/products/products_triton_tl_3.asp

[2] C. Lohse, *et al.*, "Temporary barrier usage in work zone," UC Davis, Davis June 30 2007.

[3] American Association of State Highway and Transportation Officials (AASHTO), "Manual of assessing hardware (MASH)," ed. Washington D.C, 2009.

[4] European Committee for Standardization, "European Standard EN 1317 : Road Restraint Systems," in *Part 1-5*, ed. Brussels: Standards Policy and Strategy Committee, 1998, 2010.

[5] R. Gupta and A. D. Kelkar, "Nonlinear Crash Dynamics Simulation of Novel Airbag Based Next Generation Energy Absorbing Barrier," 2006.

[6] M. B. C. Ulker, *et al.*, "Traffic barriers under vehicular impact: from computer simulation to design guidelines," *Computer-Aided Civil and Infrastructure Engineering*, vol. 23, pp. 465-480, Aug 2008.

[7] D. Marzougui, *et al.*, "Evaluation of portable concrete barriers using finite element simulation," *Transportation Research Record: Journal of the Transportation Research Board*, vol. 1720, pp. 1-6, 2000.

[8] D. Marzougui, *et al.*, "Performance evaluation of portable concrete barriers," 2007.

[9] Roads & Traffic Authority, "Wire rope safety barrier crash test," 2004.

[10] M. Larsson, *et al.*, "Flexible barrier systems along high-speed roads: a lifesaving opportunity," Monash University Accident Research Center VicRoads, Melbourne2003.

[11] T. Pieglowski, "The influence of Wire Rope Barriers on Motorcyclists," Dept of Civil ad Environmental Engineering, Lulea University of Technology, Lulea, 2005.

[12] T. Jiang, Grzebieta, R.H., Zhao, X.L., "Determining lateral deflections of plastics water-filled barriers," in *International Crashworthiness Conference- ICRASH*, Melbourne 2002.

[13] R. Zou, *et al.*, "Development of a temporary water-filled plastic barrier system," in *International Crashworthiness Conference (ICrash), 2nd, 2000, London, United Kingdom*, 2000.

[14] G. R. Liu and Y. Gu, "Coupling of element free Galerkin and hybrid boundary element methods using modified variational formulation," *Computational Mechanics*, vol. 26, pp. 166-173, 2000.

[15] Y. T. Gu and G. R. Liu, "Meshless methods coupled with other numerical methods for solids and structures," *Tsinghua Science & Technology*, vol. 10, pp. 8-15, 2005.

[16] L. Lucy, "A numerical approach to the testing of the fission hypothesis," *The Astronomical Journal*, vol. 82, pp. 1013-1024, 1977.

[17] R. A. Gingold and J. J. Monaghan, "Smoothed particle hydrodynamics-theory and application to non-spherical stars," *Monthly Notices of the Royal Astronomical Society*, vol. 181, pp. 375-389, 1977.

[18] S. Swaddiwudhipong, *et al.*, "High Velocity Penetration/Perforation Using Coupled Smooth Particle Hydrodynamics-Finite Element Method," *International Journal of Protective Structures*, vol. 1, pp. 489-506, 2010.

[19] A. Crespo, *et al.*, "Modeling dam break behavior over a wet bed by a SPH technique," *Journal of Waterway, Port, Coastal, and Ocean Engineering*, vol. 134, p. 313, 2008.

[20] R. Chieragatti, *et al.*, "Modelling high speed machining with the SPH method," 2008.

[21] G. R. Liu and M. B. Liu, *Smoothed particle hydrodynamics : a meshfree particle method*. New Jersey: World Scientific, 2003.

[22] J. J. Monaghan, "Simulating free surface flows with SPH," *Journal of Computational Physics*, vol. 110, pp. 399-406, 1994.

[23] J. J. Monaghan, "Smoothed particle hydrodynamics," *Annual review of astronomy and astrophysics*, vol. 30, pp. 543-574, 1992.

[24] M. B. Liu and G. R. Liu, "Smoothed particle hydrodynamics (SPH): An overview and recent developments," *Archives of Computational Methods in Engineering*, vol. 17, pp. 25-76, 2010.

[25] J. Monaghan, "Smoothed particle hydrodynamics," *Reports on Progress in Physics*, vol. 68, p. 1703, 2005.

[26] M. S. Fulbright, *et al.*, "A method of smoothed particle hydrodynamics using spheroidal kernels," *The Astrophysical Journal*, vol. 440, pp. 254-262, 1995.

[27] J. Campbell, *et al.*, "A contact algorithm for smoothed particle hydrodynamics," *Computer Methods in Applied Mechanics and Engineering*, vol. 184, pp. 49-65, 2000.

[28] J. C. Campbell, *et al.*, "Modelling fluid-structure impact with the coupled FE-SPH approach," 2010, pp. 131-138.

[29] T. De Vuyst, *et al.*, "Coupling between meshless and finite element methods," *International Journal of Impact Engineering*, vol. 31, pp. 1054-1064, 2005.

[30] M. Anghileri, *et al.*, "Rigid body water impact-experimental tests and numerical simulations using the SPH method," *International Journal of Impact Engineering*, vol. 38, pp. 141-151, 2011.

[31] M. Anghileri, *et al.*, "Fluid-structure interaction of water filled tanks during the impact with the ground," *International Journal of Impact Engineering*, vol. 31, pp. 235-254, 2005.

[32] R. B. Gover, Thiyahuddin, M.I, Yan, C., Oloyede, A., Gu Y.T., , "Development of a combined FE/SPH model of a road safety barrier," presented at the 4th International Conference on Computational Methods (ICCM2012) Gold Coast, Australia, 2012.

[33] M. I. Thiyahuddin, Gu Y.T, Thambiratnam D.P, Gudimetla P.G, "Impact & energy absorption of road safety barriers by coupled SPH/FEM," *International Journal of Protective Structures*, vol. 3, p. 16, 11/09/2012 2012.

[34] Y. T. Gu and L. C. Zhang, "Coupling of the meshfree and finite element methods for determination of the crack tip fields," *Engineering Fracture Mechanics*, vol. 75, pp. 986-1004, 2008.

[35] Y. T. Gu and G. R. Liu, "A coupled element free Galerkin/Boundary Element method for stress analysis of two-dimensional solids," *Computer Methods in Applied Mechanics and Engineering*, vol. 190, pp. 4405-4419, 2001.

[36] Y. T. Gu and G. R. Liu, "Hybrid boundary point interpolation methods and their coupling with the element free Galerkin method," *Engineering Analysis with Boundary Elements*, vol. 27, pp. 905-917, 2003.

[37] P. L. Centurion Barrier Systems, "Centurion Zone Barrier Technical Details," P. L. Centurion Barrier Systems, Ed., ed. Brisbane, QLD, 2011.

[38] Transportation Research Board National Research Council, "NCHRP Report 350: Recommended Procedures for the Safety Performance Evaluation of Highway Features," ed, 1993.

[39] T. Belytschko, Lin, J.I, Tsay, C.H, "Explicit algorithms for the nonlinear dynamics of shells," *Computer Methods in Applied Mechanics and Engineering*, vol. 42, pp. 225-251, 1984.

[40] H. Lobo, "Methodology for selection of material models for plastics impact simulation," 2006.

[41] J. O. Hallquist, *LS-DYNA keyword user manual version 971*. Livermore, California, 2007.

[42] A. S. o. T. M. I. ASTM, "ASTM D638 - 10 Standard test method for tensile properties of plastics," ed. West Conshohocken, PA, 2010.

[43] A. A. o. S. Highway and T. Officials, *Manual for assessing safety hardware, 2009*: American Association of State Highway and Transportation Officials, 2009.

[44] D. T. Shane, "Development of a connection detail for Polyethylene, segmental temporary barriers, final report to ultra barrier," Midwest Roadside Safety Facility, University of Nebraska-Lincoln, Lincoln, NebraskaSeptember 27, 1993 1993.

[45] M. I. Thiyahuddin, Gu Y.T, Thambiratnam D.P, "A Coupled SPH/FEM analysis of portable water filled barriers," presented at the 4th International Conference on Computational Methods (ICCM2012) Gold Coast, Australia, 2012.

[46] P. W. Randles and L. D. Libersky, "Smoothed Particle Hydrodynamics: Some recent improvements and applications," *Computer Methods in Applied Mechanics and Engineering*, vol. 139, pp. 375-408, 1996.

[47] J. Hallquist. (1998, 2006, 2012). *LS-DYNA3D theoretical manual*.

[48] R. O. Davis, "Further comments on thermodynamic response of Mie-Gruneisen materials," *Zeitschrift für Physik B Condensed Matter*, vol. 17, pp. 63-70, 1973.

[49] D. Steinberg, "Spherical explosions and the equation of state of water," Lawrence Livermore National Lab., CA (USA)1987.

[50] B. Hammonds, Burbridge, A., O'Calaghan, N., Cassar, D., Troutbeck, R., "Observation on performance of plastics water-filled barrier type device," presented at the 25th ARRB Conference, Perth, Australia, 2012.

[51] M. I. Thiyahuddin, Gu Y.T, Thambiratnam D.P, Gover, R.B, "Safety enhancement of water-filled road safety barriers using interaction of composite materials " *International Journal of Technology*, vol. 4, p. 10, 2013.